ARTICLES

Wave-Packet-Assisted Decomposition of Femtosecond Transient Ultraviolet−Visible Absorption Spectra: Application to Excited-State Intramolecular Proton Transfer in Solution

N. P. Ernsting,* S. A. Kovalenko, T. Senyushkina, J. Saam, and V. Farztdinov

Institut für Chemie, Humboldt Universität zu Berlin, Bunsenstrasse 1, D-10117 Berlin, Germany

Received: September 16, 2000; In Final Form: January 18, 2001

Femtosecond transient absorption spectra of molecules in solution change when an ultrafast reaction creates a new product state, and coherent optical processes complicate the spectra during the pump pulse. A low-frequency vibration may also be found to modulate an absorption or emission band for the first few picoseconds. For singular value decomposition of the data one identifies the educt, intermediate, and product states by their temporal behavior and thereby determines the spectra associated with these photochemical species. Here we extend this method by introducing two additional "species": the apparatus function and the low-frequency oscillation. Associated with the apparatus function is the coherent spectrum. The spectrum of oscillations is obtained directly by optimizing a generalized rotation matrix, without need of model functions. It consists of band derivatives times oscillation amplitudes and after integration assists in decomposing the transient absorption spectra. The method is demonstrated with the excited-state intramolecular proton transfer (ESIPT) reaction of 2,5-bis(2′-benzoxazolyl)hydroquinone in tetrahydrofuran. Ultrafast optical pumping prepares the excited enol form of the molecule. Its blue stimulated emission band prior to the reaction is reported for the first time. The enol form reacts with 110 ± 15 fs time constant to the excited keto form which emits in the red. The latter is created with coherent excitation of an H-chelate-ring bending vibration of 118 cm^{-1} and the proton transfer occurs during the first half-cycle. The wave packet modulates the frequency for an excited-state absorption (ESA) band of the keto form and for its stimulated emission band, with initial frequency excursions of +130 cm^{-1} and −180 cm^{-1}, respectively. The dominant ESA band is extracted quantitatively from the data. Intramolecular vibrational redistribution in the excited keto state is characterized by vibrational dephasing (0.89 ± 0.1 ps time constant) and a red shift of the ESA band (1.26 ± 0.1 ps). The spectra of all species are obtained and decomposed.

1. Introduction

Because of advances in laser technology, optical pulses are now routinely available from the near-infrared to ultraviolet spectral regions with pulse durations below 30 fs. The dynamics of condensed matter can therefore be studied by nonlinear optical techniques in the time-domain[1] with unprecedented sophistication. In photochemistry, transient optical absorption spectroscopy is the most common tool to study ultrafast reactions of molecular systems in the condensed phase. Here one measures the absorption of a time-delayed probe pulse which is tuned to an appropriate electronic transition of the evolving system. In systems where the excited state is well-known, transform-limited probe pulses centered at a single wavelength may, in principle, suffice to monitor the nuclear dynamics.[2,3] But in reactive systems, spectral changes are more typically distributed over a frequency range exceeding 10000 cm^{-1} because several electronic states are involved in the course of large-amplitude nuclear motion. For an analysis in terms of nuclear coordinates to be feasible, several detection wavelengths covering the visible spectrum must be employed even if <10 fs pulses are used.[4] Femtosecond optical *spectroscopy* may then be achieved by recording pump/probe scans for many different probe wavelengths separately:[5−7] a spectrum at a specific delay time can be constructed from the kinetic traces if the relative amplitudes for neighboring traces are known. The latter condition presently limits the utility of this approach to femtosecond spectroscopy. In an alternative approach a femtosecond white-light pulse (the so-called "supercontinuum"[8−10]) is used to measure the transient absorption spectrum at a given delay time in a single shot.[11−17] Following the development of theory[18] and optical improvements, this pump/supercontinuum probe (PSCP) technique provides transient absorption spectra with absorbance noise below ±0.001 at ∼20 fs resolution (after deconvolution) covering the 300−900 nm range.[17]

Short pump pulses create the electronically excited state with a nonequilibrium distribution not only for the reactive coordinate but also for nuclear harmonic modes which are displaced upon excitation and whose frequencies fall within the pulse bandwidth. Thus, an oscillating wave packet is launched in the excited state (not necessarily coupled to reactive dynamics[19]) and a complementary "hole" wave packet propagates in the

* Corresponding author. E-mail: nernst@chemie.hu-berlin.de. Fax: +49-30-2093-5553.

10.1021/jp003298o CCC: $20.00
Published on Web 03/13/2001

SCHEME 1

ground state. Consider for the moment the evolving excited state only. An electronic transition originating from it will be modulated by a wave packet if the transition strength or frequency depend on the corresponding low-frequency coordinates.[2] When transient absorption is measured at a single wavelength, a signal oscillation will be recorded. Its amplitude depends on the spectral position in the vibronic band, for example it should be proportional to the band absorption derivative in the case of frequency modulation. Now imagine detection at a sufficient number of wavelengths (i.e., covering the band completely) such that the amplitude spectrum can be constructed with signal/noise comparable to the transient absorption spectrum itself. In this way another view of the modulated band is provided. If the latter overlaps with another band which is *not* modulated by the oscillation, then the two may be separated quantitatively. The wave packet is thus used to extract a partial spectrum by a "molecular lock-in" technique.

In this paper we describe a novel procedure whereby the corresponding band is extracted from transient PSCP spectra, and apply it to an excited-state intramolecular proton transfer (ESIPT) reaction. This important type of unimolecular photoreaction is often observed in organic bifunctional molecules which contain an H-donor and acceptor group in suitable proximity, as for example in 2-(2′-hydroxyphenyl)benzoxazole (cf. Scheme 1 with X = O)

In the ground state the molecule possesses a phenolic −OH group (hence is termed "enol") and an intramolecular hydrogen bond is formed with the nearby −N═ group of the benzoxazolyl moiety in unpolar environments. Electronic $S_1 \leftarrow S_0$ ($\pi\pi^*$) excitation alters the charge distribution: the excited enol form E is no longer stable so that its "normal" fluorescence is not observed; instead the labile hydrogen atom is transferred to the acceptor site and thus the "keto" form K is created in the excited state. Now the electronic ground state has high potential energy and keto fluorescence therefore occurs in the red. Hydrogen bonds are an essential structural element of nature and the transfer of a proton or a hydrogen atom along this bond is one of the most fundamental processes in chemistry. Progress in ESIPT research has been described in several reviews.[20−23] (The process is more properly described as hydrogen transfer rather than proton transfer but the latter term has been accepted in the literature.)

Wave packet motion *following* ESIPT was observed in two cases.[24,25] The wave packet is *launched*, however, directly upon optical $S_1 \leftarrow S_0$ excitation of the enol form, as evidenced by activity in a low-frequency (≈150 cm^{-1}) mode in the absorption spectra of systems like the benzoxazole in Scheme 1[26−33] and the corresponding benzotriazole.[28,29,33] The activity was assigned to an in-plane H-chelate-ring bending mode[26,30,33] which affects the distance between the reactive sites. Taken together, the following picture of the ESIPT reaction of these compounds emerges.[25] The diabatic excited enol and keto states are coupled by vibronic interaction along the X···H···N reaction coordinate.[34−36] Because the labile H atom moves much faster than the heavy nuclei, its vibrational distribution may be taken to follow the skeletal geometry adiabatically. The distribution is originally prepared in the enol well of the double minimum

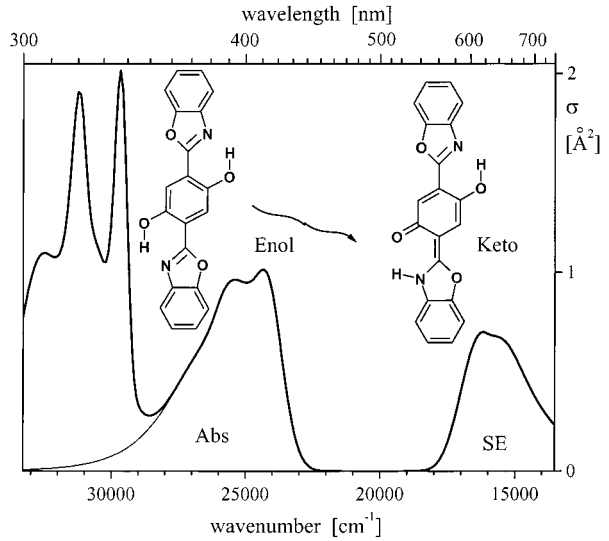

Figure 1. Absorption (Abs) and stimulated emission (SE, relative cross sections) spectra of 2,5-bis(2′-benzoxazolyl)hydroquinone in tetrahydrofuran. After optical pumping of the enol form (left), excited-state intramolecular proton transfer leads to the excited keto form (right). The vibronic envelope of the $S_1 \leftarrow S_0$ absorption band has been extrapolated into the UV and the $S_1 \rightarrow S_0$ stimulated emission band is scaled to have identical oscillator strength.

potential. But by the time that the inner turning point, i.e., the smallest X···N distance is reached, a large fraction of the population ends up in the keto product state. The effective driving force for skeletal motion is thus provided by the excited product keto state and the transfer time is of the order of half a vibrational period (≈100 fs). All previous measurements followed the rise of keto population. Blue emission from the enol form, i.e., prior to ESIPT, has never been observed in the time domain.

Here we examine 2,5-bis(2′-benzoxazolyl)hydroqinone[37−47] (BBXHQ, inset of Figure 1) which may be considered a "double" hydroxyphenyl benzoxazole.[38] Figure 1 shows its absorption and emission spectrum in tetrahydrofuran (THF) solution. BBXHQ is so far the only ESIPT compound of this type from which normal fluorescence was seen after cooling in a supersonic jet indicating that the excited enol and keto forms are nearly isoenergetic for the isolated molecule.[39] Blue enol fluorescence is also observed at room temperature in nonpolar solvents; the ESIPT reaction enthalpy in this case was estimated to be −0.5 kcal/mol.[40] In THF the fluorescence quantum yield from the primary excited enol form is orders of magnitude below that of the product keto form and the reaction may be considered irreversible in this case. Vibrational wave packets in S_1 will therefore belong essentially to the red-fluorescing, excited keto form.

With the pump/supercontinuum probe technique we measure transient absorption spectra of BBXHQ in tetrahydrofuran after 40 fs excitation at 400 nm. Following a description of the experiment, the results are presented in section 3. Data analysis by singular-value-decomposition[48−49,16] is described in section 4. The method is adapted to handle wave-packet oscillations and stimulated Raman scattering and treats convolution with the temporal apparatus function at the outset. In this way we extract the spectra which are associated with the excited enol and keto form and with the oscillations. In the discussion (section 5) these spectra are compared and bands are assigned. In particular, with the spectrum of oscillations it is possible to separate bands belonging to different optical transitions from the excited product state.

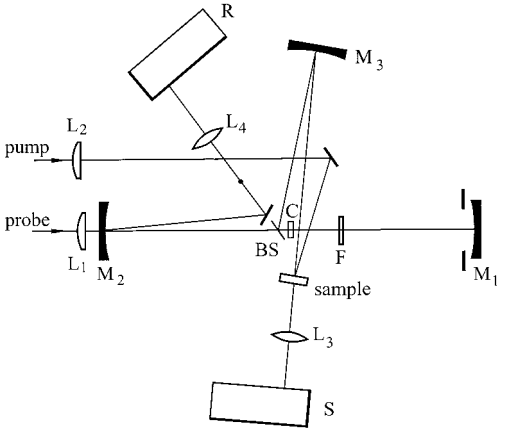

Figure 2. Experimental setup for measuring femtosecond transient absorption spectra with supercontinuum probing. The continuum is generated in a CaF_2 plate C, refocused by mirror M_1 before beamsplitter BS, and finally imaged onto the sample by M_3. Astigmatism is minimized by using mirrors off-axis in alternating planes.

2. Experimental Section

The experimental setup is shown in Figure 2. A titanium: sapphire laser system (Femtolasers) provides 30 fs, 600 μJ pulses. This basic beam is split into two parts. One part is frequency doubled and provides pump pulses centered at 396 nm. The other part (attenuated to 20 μJ pulses) forms the probe beam which is used to generate the supercontinuum in multiple filaments. The probe beam enters the setup from below, sloping upward. A lens (L_1, $f = 200$ mm) focuses the probe beam just before a 2 mm thick CaF_2 plate (C) to generate the supercontinuum which is spectrally flattened by a homemade thin filter (F). Spherical mirrors (M_1-M_3, $R = 200$, aperture 50 mm) with UV-enhanced aluminum coating image the continuum source onto the sample cell with 1.2× magnification. The first mirror is used off-axis in the meridional plane, and the other mirrors are off-axis in the sagittal plane; in this way the astigmatism of the total setup is minimized. A thin beam splitter (BS) is placed behind the intermediate waist; the reflected part is used for probing while the transmitted part is used for reference. The supercontinuum probe beam has a diameter 80−100 μm on the sample with pulse energy <0.3 μJ. The pump beam passes a variable delay stage and is then focused onto the probed sample area with a lens (L_2, $f = 500$ mm) to a diffraction-limited diameter of 120 μm. The pump pulse energy is typically 0.6 μJ. The pump and probe beams intersect at the sample with an angle of 5°. For the present measurements the pump and probe polarizations are kept parallel. The sample cell consist of fused silica windows (0.16 mm thick) spaced 0.3 mm apart and the solution is flown out of the interaction region after each shot. The transmitted probe beam and the reference beam are imaged 1:1 with short focal-length lenses (L_3 and L_4, biconvex from fused silica, $f = 25$ mm, antireflection-coated for the UV) onto the entrance plane of home-built spectrographs for sample (S) and reference (R). After alignment and spectral calibration the entrance slits are removed in order to avoid inequivalent spatial treatment of the two beams, at the cost of resolution in the UV. Each spectrum is registered on a photodiode array with 512 pixels (Hamamatsu). In the present setup the readout rate of the arrays is limited to ca. 100 Hz; this is why a mechanical chopper reduces the kHz pulse repetition rate to 30 Hz for the pump beam and to 60 Hz for the probe beam. The pump-induced optical density ΔOD is measured by comparing sample and reference signals, both with and without optical pumping, and the independence of the spectra (after appropriate normalization) from the pump pulse energy is checked.

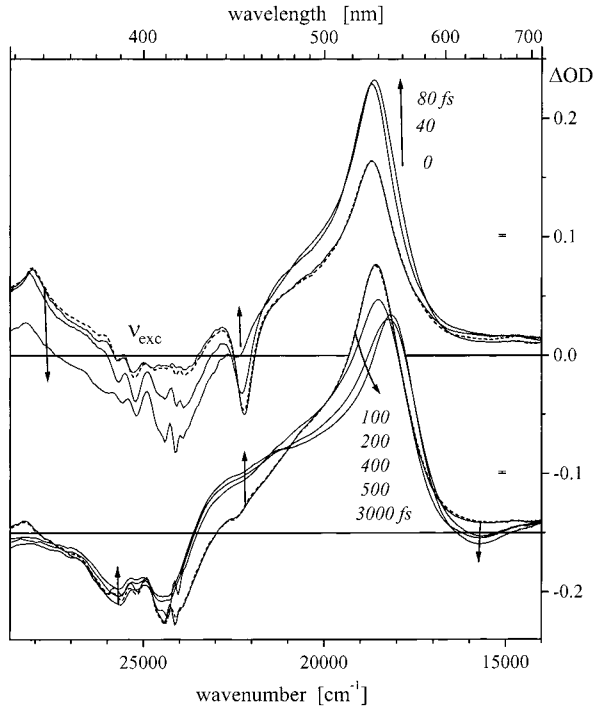

Figure 3. Transient absorption spectra (induced optical density ΔOD) of BBXHQ in THF at several delay times *t*. Spectra for $t \geq 100$ fs are shown offset by −0.15. Excited-state absorption (ESA) causes the strong induced absorbance in the visible. The standard deviation for ΔOD is ±0.0015. Simulated spectra (from rhs of eq 13) for delays of 0 and 100 fs are shown as dashed lines for comparison.

BBXHQ[37] was recrystallized repeatedly from methanol; the solvent tetrahydrofuran (THF, Merck Uvasol) was used as received. Fluorescence spectra were recorded on a fluorometer (Spex 212) which was calibrated against a secondary emission standard. Transient absorption measurements were performed at room temperature with 10 fs time steps up to 4 ps probe delay, averaging 35 measurements per step. Because the supercontinuum is chirped, a time correction must be applied to the measured kinetic trace at every probe wavelength. For this purpose we measured the nonresonant signal from the pure solvent.[18] The pump/probe intensity cross correlation is then derived from the electronic response at every probe wavelength λ. For $\lambda \geq 350$ nm it is described by a Gaussian apparatus function with width $\tau_{fwhm} = 76$ fs. (τ_{fwhm} deteriorates to 130 fs at $\lambda = 300$ nm.[50] The kinetic analysis below therefore only considers the restricted range 350 nm $\leq \lambda \leq$ 714 nm.) A root mean-square ΔOD baseline noise of 0.0015 for the transient spectra is determined at negative delay.

3. Results

Time-corrected transient absorption spectra and their evolution are presented in Figure 3. The upper part refers to delay times 0−80 fs when pump and probe pulses still overlap; the evolution after 100 fs can be seen in the lower part (i.e., offset on the ordinate. Spectra are always presented linear in probe energy although our measurement is linear in wavelength.) Comparing with Figure 1 we recognize the characteristic $S_1 \leftarrow S_0$ absorption band, but inverted due to ground-state bleaching, while negative ΔOD in the red region around 16000 cm^{-1} signifies stimulated keto emission $S_1 \rightarrow S_0$ at late times. However the dominant feature at all times is excited-state

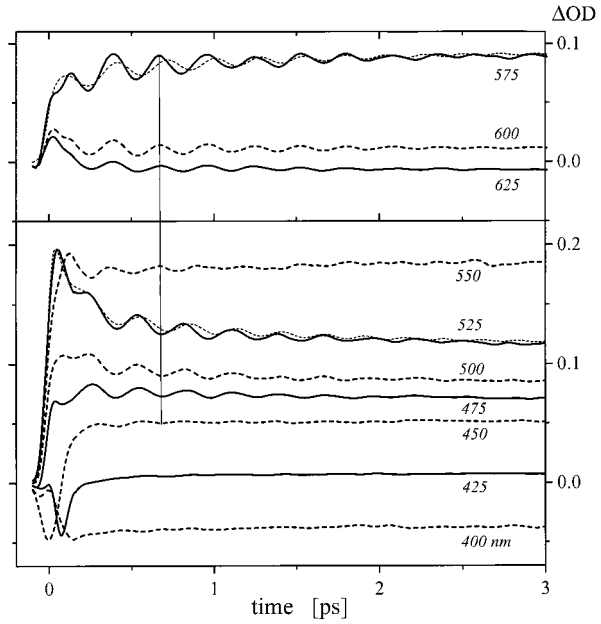

Figure 4. Kinetic traces for selected probe wavelengths. Oscillations correspond to a 118 cm^{-1} molecular vibration, with a π phase difference as indicated between traces on the red (top panel) and blue (bottom) side of the dominant ESA band. Simulated kinetic traces (from rhs of eq 13) for observation at 575 and 525 nm are shown as dashed lines for comparison.

absorption which is responsible for positive optical density in the visible range. Let us first consider delay times ≤ 80 fs (upper part): the signal builds up with a prominent ESA peak at 18900 cm^{-1} and decreases at $\nu \geq 23000$ cm^{-1} as population is removed from S_0. Positive ΔOD in the UV at $t = 0$ is largely caused by a broad background which follows the pump/probe intensity crosscorrelation as do the sharp bands at the excitation frequency $\nu_{exc} = 25250$ cm^{-1} and at 22100 cm^{-1} (cf. section 4). The background and sharp bands are coherent effects due to electronic response and stimulated Raman scattering, respectively, by the solvent.[18] The sharp 22100 cm^{-1} band is displaced from ν_{exc} by 3150 cm^{-1}, is also seen in the pure solvent, and therefore represents a C−H stretching mode of tetrahydrofuran. The corresponding inverse Raman band at 28400 cm^{-1} has the role of pump and probe fields exchanged. Next the evolution after 100 fs is discussed (lower part) which is free of coherent effects. Correlated change on a 100 fs time scale is now observed in three regions: the signal rises just to the red of the bleached absorption band (21000−24000 cm^{-1}), the ESA peak at 18900 cm^{-1} is reduced and shifts to 18000 cm^{-1}, and the keto emission around 16000 cm^{-1} appears. Further spectral change, for example the signal increase in the bleached absorption band, evolves on a picosecond time scale.

Kinetic traces for selected probe frequencies are shown in Figure 4. They reveal oscillations with a period of 280 fs corresponding to a vibrational frequency of 118 cm^{-1}. Amplitude and phase depend on the probe frequency relative to the prominent ESA peak: amplitudes are largest on either side and "red" and "blue" traces have opposite phase. Thus, it appears that the spectral position of the ESA band is modulated. For a better view of the modulation, the measured data are shown in Figure 5a as a function of probe frequency and delay time in a (smoothed) contour plot. Note that the spectral modulation can even be seen by the contour line near 22800 cm^{-1} where the transient absorption spectra are relatively flat. The stimulated Raman structure during pumping and the accumulated signal of ground-state bleaching and excited-state absorption are also

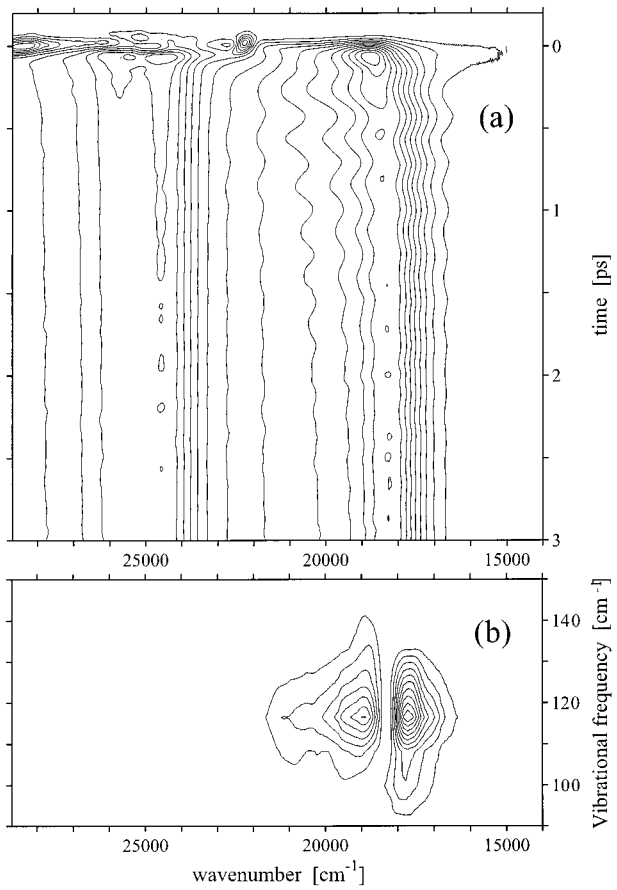

Figure 5. (a) Contour plot of the transient absorption spectra (smoothed) showing oscillations of the ESA band. (b) Fourier transform (imaginary part, $t \geq 100$ fs) of residuals from a multiexponential fit to the kinetic traces, depending on probe wavenumber.

recognized. The kinetic traces were each fitted with a multiexponential function; the lower panel (Figure 5b) shows the time Fourier transforms of the residuals as a function of probe frequency. Because of the coherent structure and other fast changes at early time, this kind of Fourier analysis had to be restricted to delay times t ≥ 100 fs; otherwise the vibrational map in Figure 5b is much distorted. On the other hand, leaving out the oscillations at earliest times in describing the signal introduces systematic errors (as is evident from Figure 5a): changes are ascribed to fast irreversible photochemistry which should rather be associated with reversible—on this time scale—spectral change. Clearly a global analysis would be useful which incorporates coherent effects, spectral modulation, and overdamped spectral evolution in a consistent and flexible way with as few assumptions as possible.

4. Data Treatment

In this section the educt, intermediate, and product states are identified by their temporal behavior and singular value decomposition[48,49] (SVD) of $\Delta OD(\lambda,t)$ is used to determine the spectra associated with these photochemical species. We extend this method by introducing two additional "species": the apparatus function and the low-frequency oscillation. Associated with the apparatus function is the coherent spectrum. The spectrum of oscillations is obtained directly, without explicit model functions, by optimizing a generalized rotation matrix. It consists of band derivatives times oscillation amplitudes and after integration assists in decomposing the transient absorption spectra.

The induced optical density at observation wavelengths λ_i ($i = 1, M$) and delay times t_j ($j = 1, N$) comprise a data matrix $\mathbf{A} \equiv \Delta OD(\lambda_i, t_j)$. For example, of the full spectral range we consider 452 equally spaced wavelengths from 350 to 714 nm and the delay time runs from -0.1 ps to 3.81 ps in 10 fs steps; hence, $\mathbf{A}$ is dimensioned 452×392. By SVD[48] the data can be written as

$$\mathbf{A} = \mathbf{USV}^{\mathrm{T}} \tag{1}$$

where the columns of $\mathbf{U}$ represent normalized basic spectra, the rows of $\mathbf{V}^{\mathrm{T}}$ contain their normalized dynamics, and diagonal $\mathbf{S}$ may be presumed to have the weights or singular values $S_{kk} > 0$ arranged in descending order. Usually just a few (say K) such combinations adequately describe the measurement; this is why after SVD the matrices $\mathbf{U}$, $\mathbf{S}$, and $\mathbf{V}^{\mathrm{T}}$ are truncated to dimensions $M \times K$, $K \times K$, and $K \times N$, respectively. (In our case $K = 4$ is sufficient as will be shown later.) A feature of femtosecond measurements is that, in every kinetic trace, oscillations may be present at several frequencies. Consider one of these. In a first step the corresponding *oscillations are concentrated on a single trace* (for example the Kth) by a generalized $K \times K$ rotation matrix $\mathbf{R}$:

$$\mathbf{A} = \mathbf{USR}^{-1}\mathbf{RV}^{\mathrm{T}} \tag{2}$$

$\mathbf{R}$ may be built up successively. The rows of $\mathbf{V}^{\mathrm{T}}$ are Fourier transformed, the spectral density is noted, and that row $m < K$ is selected for which the vibrational line at the desired frequency is largest. Then a 2×2 rotation $\mathbf{R}_1$ between rows m and K is set up and the rotation angle is optimized by maximizing the target spectral density of row K in $\mathbf{R}_1\mathbf{V}^{\mathrm{T}}$. This procedure is again applied to the optimized $\mathbf{R}_1\mathbf{V}^{\mathrm{T}}$ etc. until convergence is achieved. Altogether the rotation matrix in (2) becomes $\mathbf{R} = \mathbf{R}_n ... \mathbf{R}_2 \mathbf{R}_1$. The matrix

$$\mathbf{Q} = \mathbf{USR}^{-1} \tag{3}$$

then contains in its Kth column the amplitude of the oscillation depending on probe wavelength. The entire kinetics reside on

$$\mathbf{W} = \mathbf{RV}^{\mathrm{T}} \tag{4}$$

In the present case, modulation at only one vibrational frequency is observed and the first K-1 rows of $\mathbf{W}$ are therefore devoid of any further oscillations. (For simplicity we defer the treatment, which follows naturally, of the general case when several vibrations are associated with different electronic transitions.) At this stage the empirical part of the analysis is completed. Note that the use of a rotation in eq 2 reorganizes the overall fitting procedure of time traces to practical advantage: the spectrum of oscillations is obtained independent from photochemical kinetics and the analysis of the latter is largely decoupled from the fit of oscillations (see after eq 10).

The *analysis of the kinetics* (rows of $\mathbf{W}$) follows next. It is guided by a model for the reaction. For example imagine state-to-state kinetics whereby the primary excited enol form E decays, irreversibly, to a keto state K* which is characterized by a nonequilibrium vibrational distribution. Finally, intramolecular vibrational redistribution leads to the relaxed keto form K. This process must also be irreversible. The corresponding rate constants are k_1 and k_2:

$$\mathrm{E} \xrightarrow{k_1} \mathrm{K}^* \xrightarrow{k_2} \mathrm{K} \tag{5}$$

The coupled rate equations for the concentrations have the solution

$$\begin{bmatrix}[\mathrm{E}]\\ [\mathrm{K}^*]\\ [\mathrm{K}]\end{bmatrix}(t) = \begin{bmatrix}0 & 1 & 0\\ 0 & -k_1/(k_1-k_2) & +k_1/(k_1-k_2)\\ 1 & +k_2/(k_1-k_2) & -k_1/(k_1-k_2)\end{bmatrix}\begin{bmatrix}1\\ \exp\{-k_1 t\}\\ \exp\{-k_2 t\}\end{bmatrix} \tag{6}$$

where at $t = 0$ $[\mathrm{E}] = 1$ and $[\mathrm{K}^*] = [\mathrm{K}] = 0$ was assumed. For a description of the kinetic traces, the standard practice[49] must be extended to include convolution with the temporal apparatus function[16] and, as novel features, coherent effects and molecular vibrations. We therefore employ a column vector function $\vec{T}(t)$ which collects L temporal functions (here $L = 5$):

$$\vec{T}(t) = \begin{bmatrix}\mathrm{G}(d, t)\\ \mathrm{CH}(d, t)\\ \mathrm{CExp}(k_1, d, t)\\ \mathrm{CExp}(k_2, d, t)\\ \mathrm{CSin}(k_s, \omega_s, d, t)\end{bmatrix} \tag{7}$$

Here the Gaussian G takes care of coherent signal, the convoluted Heaviside function CH and convoluted exponentials CExp are needed for the state-to-state kinetics, and the convoluted sine function CSin describes the oscillation:

$$\mathrm{G}(d,t) \equiv 1/\sqrt{2\pi}d \exp\{-t^2/2d^2\} \tag{8a}$$

$$\mathrm{CH}(d,t) \equiv {}^1/_2 \,\mathrm{Erfc}\{-t/\sqrt{2}d\} \tag{8b}$$

$$\mathrm{CExp}(k,d,t) \equiv {}^1/_2 \exp\{k^2d^2/2 - kt\}\,\mathrm{Erfc}\{(kd^2 - t)/\sqrt{2}d\} \tag{8c}$$

$$\mathrm{CSin}(k,\omega,d,t) \equiv -i/2\,(\mathrm{CExp}(k-i\omega,d,t) - \mathrm{CExp}(k+i\omega,d,t)) \tag{8d}$$

The same set is needed for the kinetic scheme when E quickly relaxes into equilibrium with K* which then both decay slowly to K. When the values for the parameters are given, the temporal functions are tabulated for the delay times t_j to give an $L \times N$ matrix

$$\mathbf{T} = (\vec{T}(t_j)) \tag{9}$$

Now the K rows of $\mathbf{W}$, i.e., essentially the observed kinetic traces, should be expressed as linear combinations of the L rows in $\mathbf{T}$:

$$\mathbf{W} \approx \mathbf{FT} \tag{10}$$

The matrix $\mathbf{F}$ of coefficients has in its last (Lth) column only one nonzero entry: in the lowest (Kth) row, because on $\mathbf{W}$ the observed oscillations had been concentrated there exclusively. The coefficients in $\mathbf{F}$ and the parameters k_1, k_2, in $\mathbf{T}$ must be optimized simultaneously in eq 10. For this we alternate least-squares fitting of the coefficients for fixed parameters with the downhill simplex algorithm for the parameters.[48] Thereafter the spectra which are associated with the temporal functions in $\vec{T}(t)$ are the columns of

$$\mathbf{B} = \mathbf{QF} \tag{11}$$

The last step involves the *kinetic model* explicitly. All models consistent with the temporal functions may readily be examined here, for example, (5) and (6). However, in femtosecond spectroscopy, the "species" to be considered are not only the

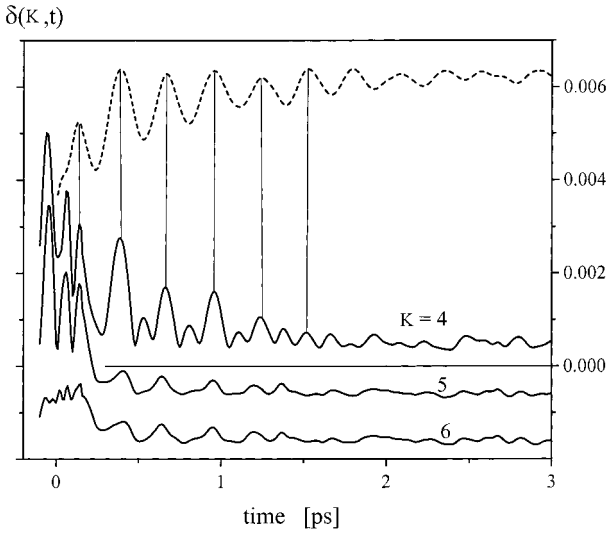

Figure 6. Error $\delta(K,t)$ incurred when representing measured transient spectra by SVD matrices truncated to K basis functions (see text). The curves for $K = 5$ and 6 are offset vertically by -0.001 and -0.002, respectively. For comparison, the experimental kinetic trace at 575 nm from Figure 4 has also been entered (scaled; dashed line).

molecular states E, K*, K but also the "pulse" G which has the spectrum of coherent effects, or the "oscillation" CSin. (The spectrum of the latter was already located in the last column of **Q**.) Therefore, the 3×3 matrix **m** in (6) must be extended to form the model matrix

$$\mathbf{M} \equiv \begin{bmatrix} 1 & & \\ & \mathbf{m} & \\ & & 1 \end{bmatrix} \tag{12}$$

When $\mathbf{M}^{-1}\mathbf{M}$ is inserted into the right-hand side of (10), the data are approximated as

$$\mathbf{A} \approx \mathbf{ZK} \tag{13}$$

where the species-associated spectra (SAS) are given by the columns of

$$\mathbf{Z} = \mathbf{BM}^{-1} \tag{14}$$

and the kinetics of the species are given by the rows of

$$\mathbf{K} = \mathbf{MT} \tag{15}$$

Let us now apply the procedure outlined above to the transient absorption spectra of BBXHQ which were already collected in the data matrix **A**. Following SVD (eq 1) the number K of independent basis spectra must first be assessed. For this purpose we compare the approximated spectrum at delay time t_j, i.e., $A_{ij}^{(K)} \equiv \Delta\mathrm{OD}^{(K)}(\lambda_i,t_j)$, with the observed one by their root mean-square distance $\delta(K,t_j) = \sqrt{\sum_{i=1}^{M}(A_{ij}^{(K)}-A_{ij})^2/M}$. In Figure 6 this representation error is plotted against time for $K = 4$, 5, and 6. We see that the transient spectra can be approximated as a weighted sum of only four spectral basis functions to better than the rms noise level of 0.0015 for most delay times (solid line in the figure) with notable exceptions during the initial interval $t \leq 200$ fs and at regular spikes afterward. With $K = 5$, the latter disappear below noise but the representation at early time is not improved, for which $K = 6$ is required. Further insight is afforded by comparison with the kinetic traces shown before, for example the one observed at 575 nm which is also entered in Figure 6. We find that the $K = 4$ spectral expansion fails significantly whenever the wave-packet-modulated spectrum reaches its redmost turning point. This kind of truncation error is typical for SVD of oscillating transient spectra as will be explained in the following.

Consider a molecular absorption band ϵ which maintains its spectral shape but has its center frequency $\langle\tilde{\nu}\rangle_t = \langle\tilde{\nu}\rangle_0 + \mathrm{d}\tilde{\nu}(t)$ modulated in time as $\mathrm{d}\tilde{\nu}(t) = \Delta\tilde{\nu}\sin(\omega,t)$ With spectrographs one registers a spectral shift $\mathrm{d}\lambda(t) = (\partial\lambda/\partial\tilde{\nu})\mathrm{d}\tilde{\nu}(t)$ for every observation wavelength; therefore

$$\Delta\mathrm{OD}(\lambda,t) = \epsilon(\lambda) - \frac{\partial\epsilon(\lambda)}{\partial\lambda}\mathrm{d}\lambda(t) - \frac{1}{2}\frac{\partial^2\epsilon(\lambda)}{\partial^2\lambda}\mathrm{d}\lambda(t)^2 - \ldots$$

$$= \epsilon(\tilde{\nu}) - \frac{\partial\epsilon(\tilde{\nu})}{\partial\tilde{\nu}}\Delta\tilde{\nu}\sin(\omega\mathrm{t}) - \frac{1}{2}\left[\frac{\partial^2\epsilon(\tilde{\nu})}{\partial\tilde{\nu}^2} + 2\frac{\partial\epsilon(\tilde{\nu})}{\partial\tilde{\nu}}/\tilde{\nu}\right]\Delta\tilde{\nu}^2\sin^2(\omega\mathrm{t}) - \ldots \tag{16}$$

On the other hand, with SVD analysis one describes a spectral oscillation by basis spectra and their associated dynamics (for example as in eq 13), and second or even higher order expansion terms in eq 16 may be required. With this background we now return to the BBXHQ data and discuss the representation error (Figure 6) as the basis set is truncated. For $K = 4$ the oscillations are well described for most of the time—as will be demonstrated later—which suggests that $\partial\epsilon/\partial\tilde{\nu}$ is captured. Therefore, the spikes of $\delta(K = 4,t)$, which occur most notably whenever the red spectral turning point is reached but are also evident between, must signify that the first four basis spectra do not adequately present the second-order spectrum [. . .] in eq 16. But ignoring this second-order term should only affect the *representation* of spectral oscillations and not their *information content* which is already embodied in the first-order spectrum. In this particular case, therefore, we truncate to $K = 4$ because it is physically justified, providing the same information as $K = 5$, but by comparison reduces the number of fitting parameters considerably.

Next, for our data only two rotations $\mathbf{R}_i$ (between rows 2 and 4 and then 3 and 4) need be optimized to sweep the oscillations into the lowest (fourth) row of **W**, and the latter is subjected to kinetic analysis, i.e., fitted according to eq 10. Note that although only four independent basis spectra and basis dynamics are admitted, the latter are described by five temporal functions (therefore **F** is dimensioned 4×5). From the fit we find the best parameters in eq 7: they are the time constants $1/k_1 = 110 \pm 15$ fs and $1/k_2 = 1.26 \pm 0.1$ ps, the oscillation decay time $1/k_s = 0.89 \pm 0.1$ ps, and the angular frequency $\omega_s = 22.2 \pm 0.1$ ps^{-1} corresponding to 118 cm^{-1}. One may now judge the quality of the approximations together with the fit. For example, the simulated transient spectra for a delay of 0 and 100 fs are shown in Figure 3 as dashed lines. Simulated kinetic traces for observation at 575 nm and at 525 nm are similarly shown in Figure 4. Here we note a shifting mismatch of observed oscillation peaks by the simulated peaks. This error was traced to the nonlinearity of the delay stage. Also the modulation amplitude is not fully reproduced by the simulated traces, most notably in the red at 575 nm, because the Taylor expansion eq 16 was limited to the first order, as was discussed above.

At this stage we adopt the model of irreversible proton transfer in the excited state (eq 5), build the model matrix (eq 12) and arrive at five species with their associated spectra and dynamics. Figure 7 shows the simulated kinetics for the primary excited enol form E (thick dashed line), the nonequilibrium keto form K* and the relaxed keto form K (thick solid lines). The temporal apparatus function is also shown (thick solid line

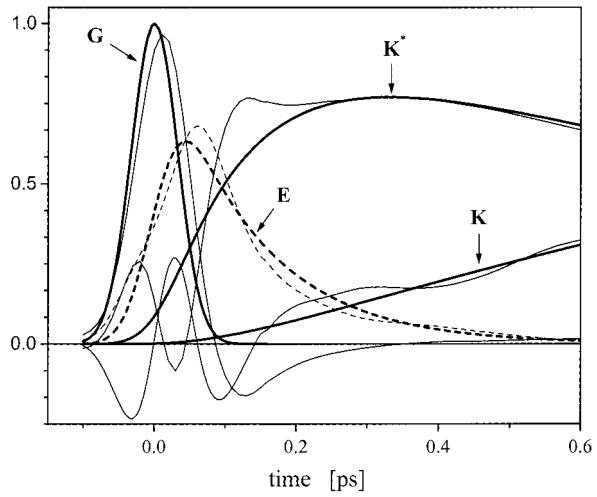

Figure 7. Species-associated kinetics for irreversible intramolecular proton-transfer E → K* → K in the excited singlet state. Here E is the primary excited enol form, K* the keto form immediately after the reaction, and K is the excited keto form after intramolecular vibrational redistribution in the excited state. G indicates the temporal apparatus function. Thick lines represent simulated curves and thin lines are used for transformed data curves (See text. Here and in the following figures, dashed lines are always used for E.) The oscillation between the experimental K* and K curves does not disqualify the simulation because the K* and K spectra are similar.

indicated G). These simulated curves were obtained by following the rhs of eq 10. If instead the same transformations are applied to the dynamical data on the lhs one obtains the experimental kinetic curves. The latter are entered as thin lines in the figure but we defer their discussion for the moment. The species-associated spectra are shown in the top panel of Figure 8. For convenience the spectra will also be termed G, E, K*, K. The last column[52] of **Z** (eq 14) contains the amplitudes for the 118 cm^{-1} oscillation which modulates the spectral position of the dominant K* ESA band (cf. Figure 5a). The process K*→K will be interpreted as intramolecular vibrational redistribution because the K* and K spectra are quite similar. A consequence of this near-degeneracy can be seen in Figure 7: the experimental traces show that the role of K and K* are exchanged during the pump pulse and shortly afterward. This is caused by optical coherent effects which are not completely compensated and therefore interfere with the spectral assignment. However, the quality of the data description is not affected.

For completeness we also examine a model when the primary excited enol E relaxes very fast into equilibrium (forward and backward rate constants f_1 and b_1, respectively) with a hot keto state K* followed by slow conversion to cold K (rate constant f_2):

$$\mathrm{E} \underset{b_1}{\overset{f_1}{\rightleftharpoons}} \mathrm{K}^* \xrightarrow{f_2} \mathrm{K} \tag{17}$$

The corresponding system of rate equations for the concentrations, again with initial conditions [E] = 1 and [K*] = [K] = 0, has the solution Here k_1 and k_2 are the parameters from the

$$\begin{bmatrix}[\mathrm{E}]\\ [\mathrm{K}^*]\\ [\mathrm{K}]\end{bmatrix}(t) = \begin{bmatrix}0 & \alpha & (1-\alpha)\\ 0 & -\alpha - k_2/(k_1-k_2) & \alpha + k_2/(k_1-k_2)\\ 1 & +k_2/(k_1-k_2) & -k_1/(k_1-k_2)\end{bmatrix} \begin{bmatrix}1\\ \exp\{-k_1 t\}\\ \exp\{-k_2 t\}\end{bmatrix} \tag{18}$$

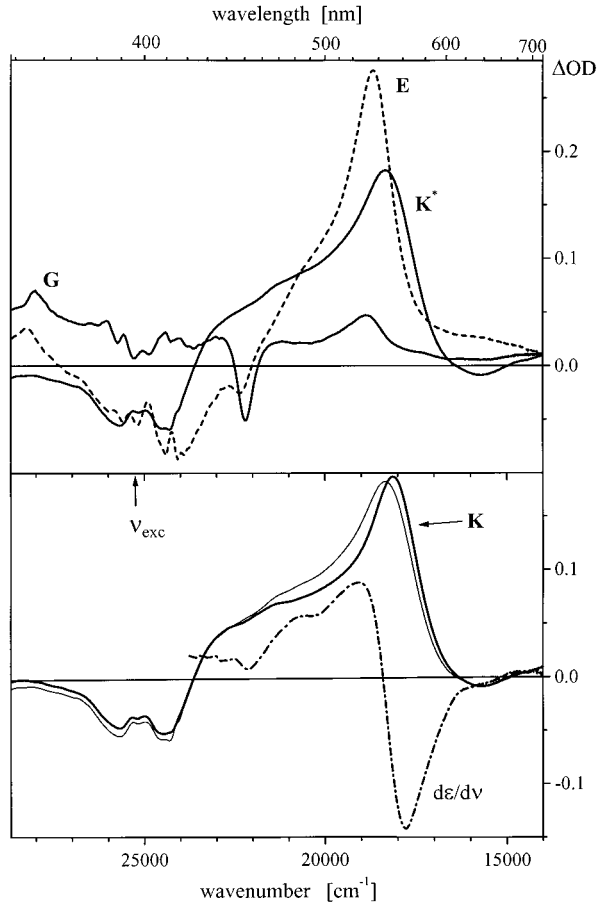

Figure 8. Species-associated spectra (SAS) for model E → K* → K of irreversible intramolecular proton transfer in the excited singlet state. G indicates the SAS of the pulse, representing stimulated Raman scattering and electronic response from the solvent. In the lower panel, the dashed−dotted line gives the SAS of the 118 cm^{-1} oscillation (×8.6), and the K* spectrum is reproduced as a thin line for comparison.

kinetic fit which determine the rate constants by

$$f_1 = \alpha(k_1 - k_2) + k_2 \tag{19a}$$

$$b_1 = (\alpha - 1)\alpha(k_1 - k_2)^2/f_1 \tag{19b}$$

$$f_2 = k_1 k_2 / f_1 \tag{19c}$$

The remaining parameter α cannot be obtained from the biexponential fit. (Note that α = 1 recovers model (5)). We set α by requiring some reasonable value for the enol → keto reaction free enthalpy

$$hc\Delta\tilde{\nu} = -RT \ln\{f_1/b_1\} \tag{20}$$

The analysis results are then recast simply by using the matrix in eq 18 for **m** in eq 12. Figure 9 shows the corresponding SAS and kinetics for $\Delta\tilde{\nu} = -240$ cm^{-1} which gives $1/f_1 = 175$ fs, $1/b_1 = 551$ fs, and $1/f_2 = 0.92$ ps.

The coherent signal was already mentioned when the earliest transient spectra (delay < 80 fs, upper part in Figure 3) were described. Within our method its spectrum is extracted from the transient data and is also plotted (G) in Figures 8 and 9. Now a broad background is exposed which is caused by electronic solvent response in combination with the chirp of the supercontinuum;[18] an increase with probe frequency reflects the dependence of the hyperpolarizability. The strong bands at 22100 and 28400 cm^{-1} were already assigned to stimulated

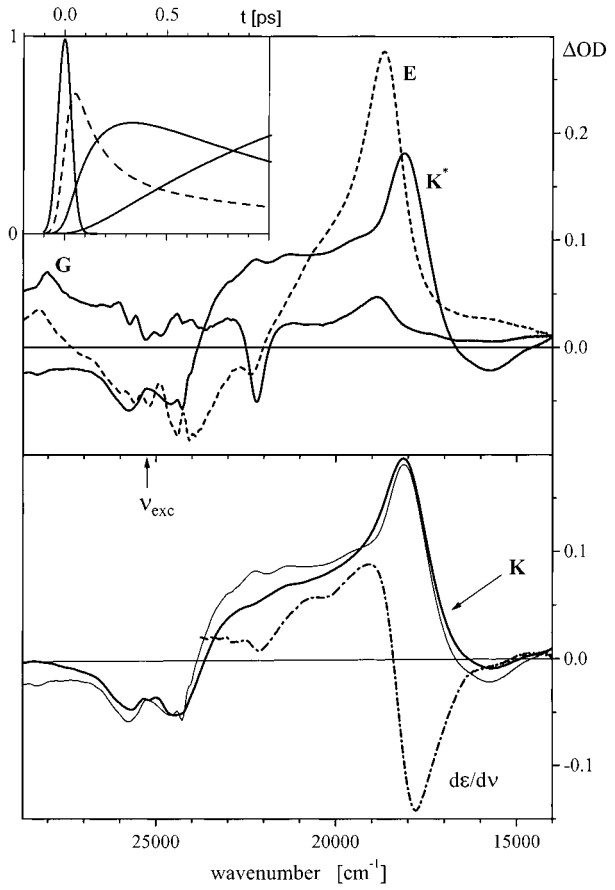

Figure 9. SAS as in Figure 8 but for model E ↔ K* → K (cf. text) of intramolecular proton transfer toward equilibrium. The kinetics is given in the inset.

Raman scattering from a solvent mode. Spectral structure around the excitation frequency with comparatively small amplitude should be assigned to resonance Raman scattering by the solute. The band around 18680 cm^{-1}, however, resembles enol excited state absorption and is not readily explained. Assignment to two-photon absorption is ruled out because the corresponding cross section involves electronic dephasing and therefore should be much smaller compared to sequential or Raman cross sections. Instead we consider this band to be an artifact caused by the description of electronic solvent signal as Gaussian only while its first and second derivative are also required.[18] (This problem is easily avoided if the pure solvent signal—which is always measured separately—is subtracted before the analysis. However, we intend to demonstrate the joint treatment of all contributions and therefore do not subtract the solvent background here.)

5. Discussion

The species E, K*, and K may be identified by comparing their spectra (for example in Figure 8) with predictions from quantum-chemical calculations for the electronically excited molecule. The latter provide frequencies and oscillator strengths for stimulated emission and excited-state absorption bands separately. On the other hand, transient absorption spectra present only the sum of all bands including ground-state bleaching. But additional information is provided by the spectrum of the low-frequency spectral oscillation which is observed until 2 ps. We show that it can be used to decompose the K* spectrum for the kinetic model of irreversible proton transfer. This leads to a complete description of spectral

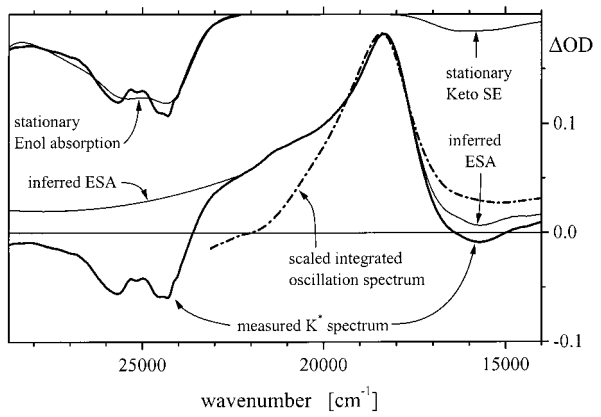

Figure 10. Decomposition of the measured K* spectrum for irreversible excited-state intramolecular proton transfer (Figure 8). The K* ESA spectrum is inferred by subtraction of the stationary absorption and keto SE bands; the latter are also shown (offset by +0.2). The dashed−dotted line results from integration of the measured spectrum of the 118 cm^{-1} oscillation followed by scaling (see text).

evolution due to excited-state intramolecular proton transfer in BBXHQ in solution in terms of observable electronic transitions.

The species-associated spectrum of K* —the keto form immediately after proton transfer in the excited state— is reproduced in Figure 10 for the model of eq 5. First, consider ground-state bleaching which is gauged quantitatively from the bleached vibronic structure at 30000 cm^{-1} (not shown in the transient spectra). The stationary $S_1 \leftarrow S_0$ absorption band, inverted and appropriately scaled, is shown offset in the upper part of the figure. We subtract this estimated bleach from the observed K* curve and thus obtain a first approximation to the ESA spectrum. The latter appears dented where the two vibronic peaks of the stationary absorption spectrum are located, and it is very probable that this structure is an artifact caused by an incorrect model for the bleached band. Therefore, the K* ESA spectrum in the blue spectral region is finally approximated by a cubic polynomial interpolation curve. Now the bleached $S_1 \leftarrow S_0$ absorption band is obtained as the difference (thick line in the offset part. The bleached vibronic structure is more pronounced compared to the stationary spectrum—an effect which we do not understand yet). The stationary keto SE spectrum is also shown offset in the upper part of the figure. Its amplitude is related to that of bleaching by the ratio of electronic oscillator strengths (0.13:0.49) from quantum-chemical calculations with the PM3 Hamiltonian.[53] Like before, we take the stationary spectrum for an estimate of the SE contribution to the measured curve, and by subtraction from the latter infer the K* ESA spectrum for the red region.

Vibrational coherence was observed at 118 cm^{-1} and the associated spectrum was presented in the previous section as a negative band derivative $\partial\epsilon/\partial\tilde{\nu}$ times amplitude $\Delta\tilde{\nu}$ for the damped spectral modulation. The underlying spectrum $\epsilon(\tilde{\nu})$ may therefore be obtained by integration followed by scaling with $f = -1/\Delta\tilde{\nu}$ and vertical shift to accommodate an integration constant. The result (scaled integrated oscillator spectrum, SIOS) is shown in Figure 10 as a dashed−dotted line. Its shape coincides with that of K* in the peak region where only excited-state absorption is expected. In fact more than one electronic transition may contribute (for example also stimulated emission) and the integrated oscillator spectrum should properly be viewed as $-\sum_i \epsilon_i(\tilde{\nu})\Delta\tilde{\nu}_i$. It follows that the oscillation amplitudes $\Delta\tilde{\nu}_i$ can be extracted if the contributing $\epsilon_i(\tilde{\nu})$ are known.

Scaling the integrated oscillator spectrum deserves some comment. We prescribe two points for the final SIOS equivalent

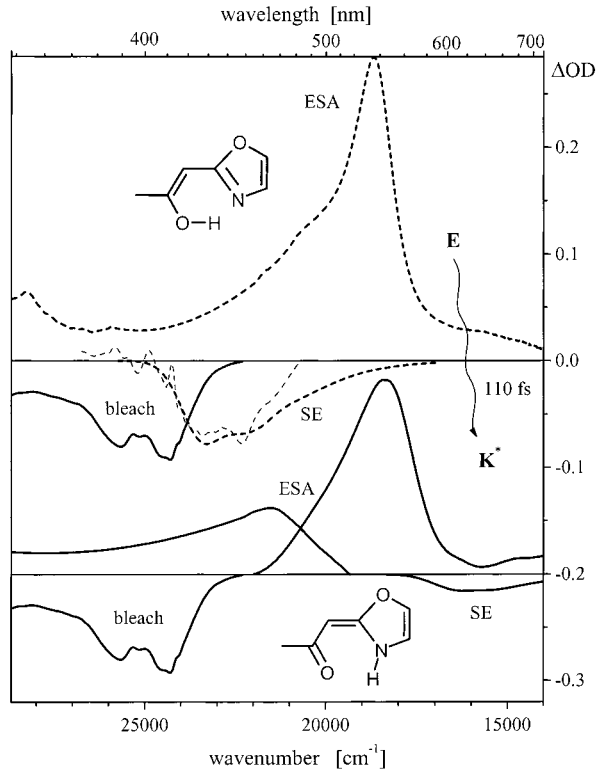

Figure 11. Decomposed transient spectra for the enol form E (upper) and the nonrelaxed keto form K* (lower part) for irreversible proton transfer. The difference between the E and K* SAS of Figure 8 is indicated as a thin dashed line.

to two assumptions. The first refers to its extremum which is taken to represent the peak of the dominant ESA transition with no contribution from neighboring transitions. The second concerns the region around 22000 cm^{-1} where the oscillation spectrum has a minimum (cf. Figure 9). Here there is no radiative coupling to the ground state for the excited keto form, bleached ground state absorption is absent, and the dominant ESA transition may safely be neglected. Then there remains just one reasonable assumption: that excited-state absorption at 22000 cm^{-1} does not oscillate so that the integrated oscillation spectrum is zero here. It follows that the integrated oscillation spectrum from 22000 cm^{-1} to the extremum at 18400 cm^{-1} presents the blue side of the dominant ESA band. When the integration result is threaded through the two prescribed points, then a scaling factor $f = -0.77 \times 10^{-2}$ cm is obtained. The various bands that together make up the K* spectrum are summarized in the lower panel of Figure 11.

The (deconvoluted) oscillation amplitudes $\Delta\tilde{\nu}_i$ will be discussed next. For the dominant ESA band we have simply $\Delta\tilde{\nu}_{ESA} = -f^{-1} = 130$ cm^{-1} because of the assumptions above. The initial excursion is directed to the blue as can be seen directly from Figure 5. Returning to Figure 10, the amplitude $\Delta\tilde{\nu}_{SE}$ for K* stimulated emission may also be estimated from the SIOS shown here. If the keto SE were not modulated, then the SIOS in the red range should retrace the dominant ESA band. But starting from the common peak toward lower energies, the inferred ESA spectrum cuts significantly below the SIOS which in this range may be written $\epsilon = \epsilon_{ESA} + \epsilon_{SE}\,\Delta\tilde{\nu}_{SE}/\Delta\tilde{\nu}_{ESA}$. Again, the transient keto stimulated emission band ϵ_{SE} is approximated by the corresponding stationary spectrum. A best fit gives $\Delta\tilde{\nu}_{SE}/\Delta\tilde{\nu}_{ESA} = -1.4 \pm 0.2$, hence $\Delta\tilde{\nu}_{SE} \approx -180$ cm^{-1} and the initial excursion of keto stimulated emission is directed to the red. A spectral amplitude is related to the dimensionless vibrational amplitude ΔQ of the wave packet by $\Delta\tilde{\nu} = \pm\tilde{\nu}_0 Q_0 \Delta Q$ for SE and ESA, respectively. Here $\tilde{\nu}_0$ is the frequency (in cm^{-1}) of the wave packet and Q_0 is the displacement of the normal mode in the final state of the transition relative to the initial state. Therefore, we have $\Delta Q_{SE}/\Delta Q_{ESA} \approx +1.4$. Concluding this discussion of spectral oscillations we point to a curious feature in Figure 5a: the contour lines on the red side of the ESA band reflect the oscillation amplitude of 130 cm^{-1} but the contour lines on the blue side have amplitude which is roughly twice as large. This may be understood with the help of Figure 11 (lower panel). Whenever the oscillating ESA band shifts to the blue, it ramps up the fixed ESA band there. The slope of the latter translates into an apparent broadening of the total ΔOD spectrum only on the blue side and thus amplifies the contour oscillation here.

The primary excited state E will be examined next, and for this we return briefly to Figure 8. The E spectrum exhibits negative induced optical density not only for the bleached absorption band but also at frequencies just below where normal fluorescence is expected. This feature therefore represents blue stimulated emission from the excited enol form. The enol SE spectrum may be derived from the absorption spectrum by assuming equal oscillator strengths, mirror symmetry for its vibronic distribution, and a reasonable location for the vibrationless transition. The enol ESA is then constructed by adding to E the ground-state bleaching and the expected enol SE spectra. After averaging over structure on a vibrational scale, the result is shown in the upper half of Figure 11 as a thick dashed line. Next, we inquire about the spectral change from E to K*. For this purpose the spectral difference E−K* is also plotted in the figure. It is seen to be similar to the enol SE, or equivalently, excited-state absorption appears to be nearly independent of the proton location in this spectral range. So the change from the E spectrum to the K* spectrum in Figure 8 directly reflects intramolecular proton transfer in the excited state. According to our knowledge, emission prior to proton transfer in such a system has thus been resolved for the first time.

In summary so far, ultrafast proton-transfer E → K* with time constant of 110 fs is seen to have the following spectral signature: (1) decay of enol SE and rise of keto SE, (2) decrease of a prominent ESA band with peak at 18680 cm^{-1} to a new one at 18340 cm^{-1}, and (3) small decrease of ESA around 28000 and 16000 cm^{-1}. The transient spectrum of K* could be decomposed with the help of the spectrum of oscillations. The dominant ESA band and the SE band of K* oscillate in opposite spectral directions with amplitudes of 130 and 180 cm^{-1}, respectively. The oscillations dephase with time constant 0.89 ps while spectral relaxation with time constant 1.26 ps consists of narrowing of the ESA peak, some reduction on its blue side and a small increase in the absorption region. Taken together, this process clearly must be assigned to intramolecular vibrational redistribution in the keto form K*.

It should be noted that the assignment of the oscillations to just one species (in our case K*) is of course required for decomposition of the corresponding SAS. For an illustration of the general problem we turn to the results with the "equilibrium" model (eq 16) as shown in Figure 9. In this case the E and K* spectra participate with fixed ratio after ca. 0.4 ps. Compared to the previous model, the measured induced optical density is now explained by longer existence of enol SE which is balanced by stronger keto ESA in that range. However the oscillatory band appears to sample the two distinct associated ESA bands and it is not clear how the pure K* ESA is to be obtained so

that the SE can be isolated. We suggest that projection of the oscillation spectrum onto the SAS be used, but to be reliable this scheme requires better signal/noise of the transient absorption measurement.

Low-frequency oscillations in the time domain[24,25] or vibronic progressions in the frequency-domain[26−32] were observed for several molecules with excited-state intramolecular proton transfer. Most recently, Riedle and co-workers[25] examined 2-(2′-hydroxyphenyl)benzothiazole (HBT, cf. Scheme 1 with X = S) in cyclohexane. Following $S_1 \leftarrow S_0$ excitation at 350 nm with 25 fs pulses, the transient absorption was probed with 20 fs pulses which were tuned to several wavelengths in the range 450−680 nm across the keto SE band. Oscillations were seen until 3 ps, with opposite phase on either side of the band, of which a 254 cm^{-1} mode is dominant. Therefore, in HBT, wave packet motion is visible by the $S_1 \rightarrow S_0$ transition of the excited keto form while in BBXHQ it is mainly seen by $S_n \leftarrow S_1$ excited-state absorption. This probably reflects different oscillator strengths for ESA vs. SE in the two molecules (remember that BBXHQ may be considered a "double" benzoxazole).

The dynamics of ESIPT is also of interest. The present study fully corroborates the concept[25] that the reaction occurs during the first half-period of an in-plane bending motion which for BBXHQ displays so prominently in the absorption spectrum.[30,31] To see this consider the mean transfer time of 110 fs, to be compared with a vibrational period of 280 fs for the active bending mode (118 cm^{-1}). In tetrahydrofuran and more polar solvents the reaction of excited BBXHQ is irreversible since the keto product state is stabilized by the solvent. In unpolar solvents like 3-methylbutane, blue emission is observed even in stationary measurements indicating thermal equilibrium between the excited enol and keto forms.[38] In this case, femtosecond transient absorption spectroscopy should reveal oscillations of the enol SE band and the equilibrium model (eq 16) must be used in order to extract the species-associated spectra. Finally, let us return to the (present) irreversible case. We modeled the reaction as a rate process, *ie.* with exponential decay for the primary excited enol form. More properly the proton-transfer should be described as coupled to the skeletal vibration in the excited state (cf. section 1). For example in HBT a delayed, steplike increase of gain was observed which points toward a 60 fs ballistic motion[25] on the pertinent skeletal coordinate which the proton- or H atom distribution follows adiabatically. This qualitative finding highlights the need to treat femtosecond wave packet modulation of optical spectra quantitatively, as begun in the present paper, including coherent signal while the pump and probe pulses still overlap. Inertial motion of population in the excited state may be included into our treatment, in a first approximation, by describing the ultrafast reaction $E \rightarrow K^*$ as a critically damped Brownian harmonic oscillator.[1]

6. Conclusion

With supercontinuum probing, femtosecond absorption experiments provide transient spectra which cover a wide frequency range (>15000 cm^{-1}). However, the spectra are the sum of contributions due to bleaching of the ground state and to stimulated emission as well as excited-state absorption from the evolving excited state. To understand a photoreaction, contributing bands must be identified and compared with results from other experiments (for example stationary fluorescence spectroscopy) or from quantum chemical calculations. To this end one can take advantage of wave packet motion in the ground or excited state which may modulate some transitions while others are unaffected. We extended the global analysis of transient spectra by singular value decomposition so that the spectrum of oscillations is extracted as part of the method. If the wave packet causes frequency modulation of an electronic transition, then the extracted spectrum is the band derivative times oscillation amplitude. The integrated oscillation spectrum is compared with the transient absorption spectrum and in this way vibronic bands and oscillation amplitudes can be obtained or related. Supercontinuum probing is advantageous here because it provides UV−vis coverage efficiently and with regular spectral spacing so that the integration can be performed numerically without spectral interpolation.

The method is demonstrated with the excited-state intramolecular proton transfer (ESIPT) reaction of 2,5-bis(2′-benzoxazolyl)hydroquinone. Ultrafast optical pumping prepares the excited enol form of the molecule. Its blue stimulated emission band prior to the reaction is reported for the first time. The enol form reacts with 110 ± 15 fs time constant to form the excited keto form which emits in the red. The latter is created with coherent excitation of an H-chelate-ring bending vibration of 118 cm^{-1} and the proton transfer occurs during the first half-cycle. The wave packet modulates the frequency for an excited-state absorption (ESA) band of the keto form and for its stimulated emission band, with initial frequency excursions of +130 cm^{-1} and −180 cm^{-1}, respectively. The dominant ESA band is extracted quantitatively from the data. Intramolecular vibrational redistribution in the excited keto state is evidenced by vibrational dephasing (0.89 ± 1 ps time constant) and a red shift of the ESA band (1.26 ± 0.1 ps). The spectra of all species are obtained and decomposed.

Acknowledgment. We are grateful to the Deutsche Forschungsgemeinschaft for support.

References and Notes

(1) Mukamel, S. *Principles of Nonlinear Optical Spectroscopy*; Oxford University Press: New York, 1994; Chapter 10 ff.
(2) Chesnoy, J.; Mokhtari, A. *Phys. Rev. A* **1988**, *38*, 3566.
(3) Yang, T.-S.; Chang, M.-S.; Chang, R.; Hayashi, M.; Lin, S. H.; Vöhringer, P.; Dietz, W.; Scherer, N. F. *J. Chem. Phys.* **1999**, *110*, 12070.
(4) Brito Cruz, C. H.; Fork, R. L.; Knox, W. H.; Shank, C. V. *Chem. Phys. Lett.* **1986**, *132*, 341.
(5) Lenderink, E.; Duppen, K.; Wiersma, D. *J. Phys. Chem.* **1995**, *99*, 8972.
(6) Thomsen, C. L.; Thogersen, J.; Keiding, S. R. *J. Phys. Chem. A* **1998**, *102*, 1062.
(7) Yamaguchi, S.; Hamaguchi, H.; *J. Chem. Phys.* **1998**, *109*, 1397.
(8) Alfano, R. R.; Shapiro, S. L. *Phys. Rev. Lett.* **1970**, *24*, 584.
(9) Shank, C. V.; Yen, R.; Fork, L.; Orenstein, J.; Baker, G. L. *Phys. Rev. Lett.* **1982**, *49*, 1660.
(10) Fork, R. L.; Shank, C. V.; Hirliman, C.; Yen, R.; Tomlinson, W. J. *Opt. Lett.* **1983**, *8*, 1.
(11) Kang, T. J.; Yu, J.; Berg**,** M. *J. Chem. Phys*. **1991**, *94*, 2413.
(12) Murakami, H.; Kinoshita, S.; Hirata, Y.; Okada, T.; Mataga, N. *J. Chem. Phys* **1992**, *97*, 7881.
(13) Nishiyama, K.; Asano, Y.; Nashimoto, N.; Okada, T. *J. Mol. Liq.* **1995**, *65/66*, 41.
(14) Eilers-König, N.; Kühne, T.; Schwarzer, D.; Vöringer, P.; Schroeder, J. *Chem. Phys. Lett.* **1996**, *253*, 69.
(15) Müller, M. G.; Hucke, M.; Reus, M.; Holzwarth, A. R. *J. Phys. Chem.* **1996**, *100*, 9527.
(16) Ruthmann, J.; Kovalenko, S. A.; Ernsting, N. P.; Ouw D. *J. Chem. Phys.* **1998**, *109*, 5466.
(17) Kovalenko, S. A.; Schanz, R.; Farztdinov, V. M.; Hennig, H.; Ernsting, N. P. *Chem. Phys. Lett.* **2000**, *323*, 312.
(18) Kovalenko, S. A.; Dobryakov, A. L.; Ruthmann, J.; Ernsting, N. P. *Phys. Rev. A* **1999**, *59*, 2369.
(19) Seel, M.; Engleitner, S.; Zinth, W. *Chem. Phys. Lett.* **1997**, *275*, 363.
(20) Arnaut, L. G.; Formosinho *S.* J. *J. Photochem. Photobiol A: Chem.* **1993**, *75*, 21.
(21) Ormson, S. M.; Brown, R. G. *Prog. React. Kinet.* **1994**, *19*, 45.

(22) Douhal, A.; Lahmani, F.; Zewail, A. H. *Chem. Phys*. **1996**, *207*, 477.
(23) Perrin, C. L.; Nielson, J. B. *Annu. Rev. Phys. Chem*. **1997**, *48*, 511.
(24) Chudoba, C.; Riedle, E.; Pfeiffer, M.; Elsaesser, T. *Chem. Phys. Lett.* **1996**, *263*, 622.
(25) Lochbrunner, S.; Wurzer, A. J.; Riedle, E. *J. Chem. Phys.* **2000**, *112*, 10699.
(26) Arthen-Engeland, Th.; Bultmann, T.; Ernsting, N. P.; Rodriguez, M. A.; Thiel, W. *Chem. Phys.* **1992**, *163*, 43.
(27) Douhal, A.; Lahmani, F.; Zehnacker-Rentien, A.; Amat-Guerri, F. *J. Phys. Chem.* **1994**, *98*, 12198.
(28) Pfeiffer, M.; Lenz, K.; Lau, A.; Elsaesser, T. *J. Raman Spectrosc.* **1995**, *26*, 607.
(29) Pfeiffer, M.; Lenz, K.; Lau, A.; Elsaesser, T.; Steinke, T. *J. Raman Spectrosc.* **1997**, *28*, 61.
(30) Ernsting, N. P. *J. Phys. Chem.* **1985**, *89*, 4932.
(31) Ernsting, N. P.; Arthen-Engeland, Th.; Rodriguez, M. A.; Thiel, W. *J. Chem. Phys.* **1992**, *97*, 3914.
(32) Vdovin, A.; Sepiol, J.; Jasny, J.; Kauffman, J. M.; Mordzinski, A. *Chem. Phys. Lett.* **1998**, *296*, 557.
(33) Pfeiffer, M.; Lau., A.; Lenz, K.; Elsaesser, T. *J. Phys. Chem.* **1997**, *268*, 258.
(34) Sobolewski, A. L.; Domcke, W. *Chem. Phys.* **1994**, *184*, 115.
(35) Sobolewski, A. L.; Domcke, W. *Chem. Phys.* **1998**, *232*, 257.
(36) Sobolewski, A. L.; Domcke, W. *J. Phys. Chem. A* **1999**, *103*, 4494.
(37) Orlando jun., C. M.; Wirth, J. G.; Heath, D. R. *Chem. Commun.* **1971**, 1551.
(38) Mordzinski, A.; Grabowska, A.; Kühnle, W.; Krowczyn, A. *Chem. Phys. Lett.* **1983**, *101*, 291.
(39) Brackmann, U.; Ernsting, N. P.; Ouw, D.; Schmitt, K. *Chem. Phys. Lett.* **1984**, *110*, 319.
(40) Mordzinski, A.; Grabowska, A.; Teuchner, K. *Chem. Phys. Lett.* **1984**, *111*, 383.
(41) Mordzinski, A.; Kühnle, W. *J. Phys. Chem.* **1986**, *90*, 1455.
(42) Dick, B. Ber. *Bunsen-Ges. Phys. Chem.* **1987**, *91*, 1205.
(43) Grabowska, A.; Mordzinski, A.; Tamai, N.; Yoshihara, K. *Chem. Phys. Lett.* **1988**, *153*, 389.
(44) Grabowska, A.; Mordzinski, A.; Kownacki, K.; Gilabert, E.; Rullière, C. *Chem. Phys. Lett.* **1991**, *177*, 17.
(45) Grabowska, A.; Sepiol, J.; Rullière, C. *J. Phys. Chem.* **1991**, *95*, 10493.
(46) Mühlpfordt, A.; Even, U.; Ernsting, N. P. *Chem. Phys. Lett.* **1996**, *263*, 178.
(47) Wortmann, R.; Lebus, S.; Reis, H.; Grabowska, A.; Kownacki, K.; Jarosz, S. *Chem. Phys.* **1999**, *243*, 295.
(48) Press, W. H.; Teukolsky, S. A.; Vetterling, W. T.; Flannery, B. P. *Numerical Recipes in Fortran*, 2nd ed.; Cambridge Univerity Press: New York, 1992.
(49) Chen, W.-G.; Braiman, M. S. *J. Photochem. Photobiol.* **1991**, *54*, 905.
(50) We find $\tau_{fwhm}/fs = 910 - 4.85\,(\lambda/nm) + 0.00896\,(\lambda/nm)^2 - 5.24\,10^{-6}\,(\lambda/nm)^3 \pm 7$ for the range $\lambda = 350-670$ nm and 76 fs is the average. Spectral change beyond 670 nm is small and does not influence the analysis which is therefore extended to 714 nm.
(51) The number of species may be larger than the number of independent basis functions (see ref 49).
(52) the 5th, proportional to the last (fourth) column of **Q** by construction.
(53) Stewart, J. J. P. *J. Comput. Chem.* **1989**, *10*, 209.